Title

Genetically targeted single-channel optical recording reveals multiple Orai1 gating states and oscillations in calcium influx.

Journal

Proceedings of the National Academy of Sciences of the United States of America, 113(2)

ISSN

0027-8424

Authors

Dynes, Joseph L
Amcheslavsky, Anna
Cahalan, Michael D

Publication Date

2016

DOI

10.1073/pnas.1523410113

Genetically targeted single-channel optical recording reveals multiple Orai1 gating states and oscillations in calcium influx

Joseph L. Dynes[a], Anna Amcheslavsky[a,1], and Michael D. Cahalan[a,b,2]

[a]Department of Physiology and Biophysics, University of California, Irvine, CA 92697 and [b]Institute for Immunology, University of California, Irvine, CA 92697

Contributed by Michael D. Cahalan, November 30, 2015 (sent for review August 9, 2015; reviewed by Richard S. Lewis and Erwin Neher)

Orai1 comprises the pore-forming subunit of the Ca^{2+} release-activated Ca^{2+} (CRAC) channel. When bound and activated by stromal interacting molecule 1 (STIM1), an endoplasmic reticulum (ER)-resident calcium sensor, Orai1 channels possess high selectivity for calcium but extremely small conductance that has precluded direct recording of single-channel currents. We have developed an approach to visualize Orai1 activity by fusing Orai1 to fluorescent, genetically encoded calcium indicators (GECIs). The GECI–Orai1 probes reveal local Ca^{2+} influx at STIM1–Orai1 puncta. By whole cell recording, these fusions are fully functional as CRAC channels. When GECI–Orai1 and the CRAC-activating domain (CAD) of STIM1 were coexpressed at low levels and imaged using a total internal reflectance fluorescence microscope, cells exhibited sporadic fluorescence transients the size of diffraction-limited spots and the brightness of a few activated GECI proteins. Transients typically rose rapidly and fell into two classes according to duration: briefer "flickers" lasting only a few hundred milliseconds, and longer "pulses" lasting one to several seconds. The size, intensity, trace shape, frequency, distribution, physiological characteristics, and association with CAD binding together demonstrate that GECI–Orai1 fluorescence transients correspond to single-channel Orai1 responses. Single Orai1 channels gated by CAD, and small Orai1 puncta gated by STIM1, exhibit repetitive fluctuations in single-channel output. CAD binding supports a role in open state maintenance and reveals a second phase of CAD/STIM1 binding after channel opening. These first recordings of single-channel Orai1 currents reveal unexpected dynamics, and when paired with CAD association, support multiple single-channel states.

CRAC channel | Orai | Stim | store-operated Ca^{2+} entry | local Ca^{2+}

In eukaryotic cells, calcium ions (Ca^{2+}) are a primary means of controlling protein-based molecular machines (1). Receptor stimulation leads to two phases of cytoplasmic Ca^{2+} signals in many cell types: a transient release of Ca^{2+} from the endoplasmic reticulum (ER) mediated by 1,4,5 inositol trisphosphate (IP_3), and a subsequent more sustained Ca^{2+} influx through ion channels in the plasma membrane (PM) (2). These two phases are linked; depletion of Ca^{2+} from the ER lumen acts as a signal to open Ca^{2+} channels in the PM. This process, called store-operated calcium entry (SOCE), is mediated by a two-component channel consisting of the pore-forming subunit, Orai, and the ER resident Ca^{2+} sensor, stromal interacting molecule (STIM) (3, 4). Upon ER Ca^{2+} store depletion, STIM translocates to ER–PM junctions, where it binds, clusters, and opens Orai channels in the PM at signaling structures called puncta. Ca^{2+} influx through Orai1 is an essential and widely used signal that initiates and regulates motility, gene transcription, and cytokine secretion and underlies adaptive immune responses (5, 6). The presence of three Orai genes (Orai1, -2, and -3) and two STIM genes (STIM1 and STIM2) with somewhat different properties contributes to the utility and diversity of this signaling mechanism.

Orai channels are unrelated to other ion channels and possess a characteristic biophysical fingerprint: a very small conductance estimated at ~10 fS (femtosiemens), 1,000-fold selectivity of Ca^{2+} over Na^{+}, conduction of monovalent cations in the absence of Ca^{2+}, and inward rectification (3, 4). Individual Orai proteins contain four transmembrane domains and in the closed state assemble as threefold symmetric hexamers (7). For gating, STIM1 binds to at least two sites on the cytoplasmic face of Orai1, strongly to a C-terminal site just after TM4 and weakly to an N-terminal site just before TM1 (3, 4). These binding sites have been mapped to an ~100 amino acid domain in STIM1, termed Ca^{2+} release-activated Ca^{2+} (CRAC)-activating domain (CAD) or STIM1 Orai activating region (SOAR), that when coexpressed opens Orai1 channels in the absence of ER store depletion (8, 9). In addition, Orai3 can be opened in a STIM-independent manner by application of 2-aminoethyl diphenylborinate (2-APB) (3, 4).

The properties of Orai1 channels, including pore size, cation permeability, conductance levels, and Ca^{2+}-dependent inactivation (CDI), vary markedly, depending upon the ratio of STIM1 to Orai1 expression in transfected cells (10–12) and in self-activating tandem Orai1–STIM1 constructs (13) These studies point to multiple conducting states triggered by STIM1 binding. The number, activation sequence, and steady-state heterogeneity of these states are central issues for understanding the function and output of Orai1. These issues might be resolved by analysis of single Orai1 channels, yet despite successes in biophysical and

Significance

Calcium ions serve as intracellular signals controlling many aspects of cell behavior. Here, we create fusions of genetically encoded calcium indicators and cell surface Orai calcium channels that report calcium influx through the channel. These fluorescent fusion proteins will allow us to see in living cells Orai signals that underlie cell functions, especially those essential for mounting an adaptive immune response. Their output is bright enough to record the intermittent openings of a single Orai channel for the first time to our knowledge. Our recordings reveal several patterns of channel activity, including oscillations. These responses help us understand Orai channels as molecular machines, and our work enables Orai calcium signals to be identified, mapped, and related to the functional systems of the body.

Author contributions: J.L.D. and M.D.C. designed research; J.L.D. and A.A. performed research; J.L.D. analyzed data; and J.L.D. and M.D.C. wrote the paper.

Reviewers: R.S.L., Stanford University School of Medicine; and E.N., Max Planck Institute for Biophysical Chemistry.

The authors declare no conflict of interest.

[1]Present address: Illumina, Inc., San Diego, CA 92122.

[2]To whom correspondence should be addressed. Email: mcahalan@uci.edu.

This article contains supporting information online at www.pnas.org/lookup/suppl/doi:10.1073/pnas.1523410113/-/DCSupplemental.

molecular characterization, the very low unitary conductance has precluded direct recording of single-channel currents.

Optical recording of channel currents offers an alternative to whole-cell patch-clamp recording. One approach involves loading cells with Ca^{2+} indicators and visualizing the influx of Ca^{2+} through well-separated single channels in the PM (14). However, it has been validated for Ca^{2+} fluxes of 100 fA (femtoamperes), ~100 times the conductance of Orai1 in 2 mM Ca^{2+} estimated from noise analysis (15). In another approach a genetically encoded Ca^{2+} indicator (GECI) was fused to a Ca^{2+} permeable ion channel, in this case the purinergic receptor P2X, where it reported channel activity in transfected cells (16). Whereas this approach, also used in a recent study of Cav2.2 channels (17), did not attempt to record from individual channels, it is attractive because of the great improvements in GECIs over the last 3–4 y (18, 19).

Here we describe the construction and characterization of fusions of genetically encoded calcium indicators with Orai proteins. These fusions report calcium influx at STIM1–Orai1 puncta in transfected cells with high dynamic range. Moreover, their brightness allows the activity of single Orai1 channels to be recorded optically by total internal reflectance microscopy. Such recordings, representing, to our knowledge, the first single-channel records for CRAC/Orai1 channel activity, provide evidence of multiple conductance states of the open channel and periodic fluctuations in Orai1 activity.

Results

Local Ca^{2+} Entry Monitored by Tethering a Genetically Encoded Ca^{2+} Indicator to Orai1. We fused fluorescent genetically encoded calcium indicators to Orai1 to detect Orai-associated calcium influx locally in the cytoplasmic nanodomain adjacent to the membrane. The GECO (genetically encoded Ca^{2+}-indicators for optical imaging) and GCaMP series of recently published, single fluorescent protein GECIs were chosen based upon their brightness, dynamic range, and K_d values for Ca^{2+} binding (18, 19). GECOs, like GCaMPs, are tripartite fusion proteins that use the Ca^{2+}-dependent binding of a C-terminally fused calmodulin to an N-terminally fused target peptide from myosin light chain kinase (M13) to drive fluorescence of a centrally positioned circularly permuted fluorescent protein. N-terminal GECO–Orai1 fusion constructs were transiently cotransfected with STIM1 into human embryonic kidney (HEK) 293A cells and imaged using total internal reflectance fluorescence (TIRF) microscopy. Transfected cells were assessed by shifting the extracellular Ca^{2+} concentration and depleting ER calcium stores using the sarcoplasmic/endoplasmic reticulum calcium ATPase (SERCA) pump blocker thapsigargin (TG). The green fluorescent G–GECO1–Orai1 exhibited diffuse expression in the basal plasma membrane (Fig. 1 *A* and *D*), which was largely unchanged by shifting between 0 mM Ca^{2+} + EGTA (0 Ca) and 2 mM Ca^{2+} (2 Ca). Addition of TG led to clustering of G–GECO1–Orai1 into puncta (Fig. 1 *B* and *E*). Readdition of extracellular Ca^{2+} (2 mM) led to an immediate, large increase in brightness of G–GECO1–Orai1, detected at puncta (Fig. 1 *C* and *F*). The fluorescence time course for the entire basal surface of the cell is shown in Fig. 1*G*; importantly, no change in G–GECO1–Orai1 signal accompanied depletion of Ca^{2+} from ER stores. Whole-cell electrophysiological recording indicated that the G–GECO1–Orai1 fusion is fully functional as a CRAC channel (Fig. S1).

Other GECI–Orai fusions functioned in a similar manner. When cotransfected with STIM1, G–GECO1.2–Orai1 and the C-terminal fusion Orai1–GCaMP6f exhibited a similar fold increase upon Ca^{2+} readdition following TG treatment (Fig. S2 *A* and *B*, respectively). Furthermore, resting human T cells exhibited similar, though smaller, changes in G–GECO1–Orai1 fluorescence in response to TG treatment and Ca^{2+} readdition (Fig. 1*H*). Membrane targeting was confirmed by confocal microscopy (Fig. S3). In

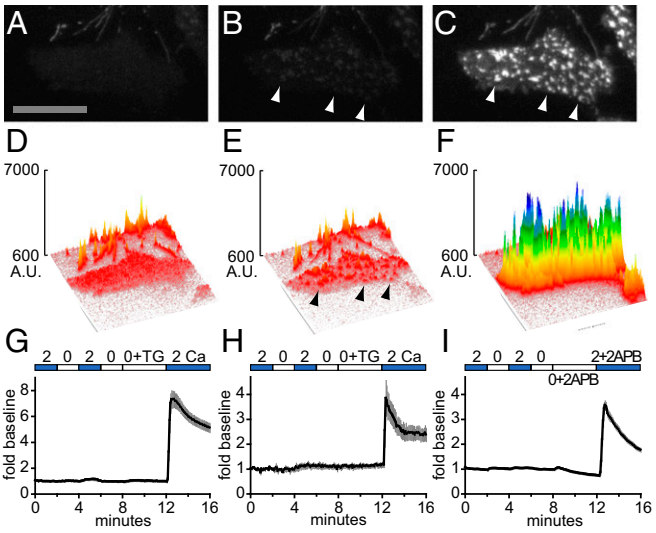

Fig. 1. GECI–Orai fusions target to puncta and report calcium influx in transfected cells. (*A–C*) TIRF micrographs of a HEK 293A cell transiently transfected with G–GECO1–Orai1 and STIM1 and imaged in 2 Ca (*A*), after 3.5 min in 0 Ca + 2 μM TG (*B*), and after shift to 2 Ca (*C*). Arrowheads indicate selected puncta. (Scale bar, 20 μm.) (*D–F*) Surface plots of the micrographs in *A–C*, respectively, indicated as arbitrary units (A.U.). Arrowheads indicate the same puncta indicated in *B* and *C*. (*G* and *H*) Time courses of G–GECO1–Orai1 plotted as mean fold baseline versus time (black lines) in HEK 293A cells (*G*; n = 26) and resting human T cells (*H*; n = 9) transiently cotransfected with STIM1 and treated with 2 μM TG. (*I*) Time course of G–GECO1–Orai3 plotted as mean fold baseline versus time (black line) in transiently transfected HEK 293A cells (n = 24) treated with 100 μM 2-APB. For *G–I*, gray bars indicate ± SEM.

fusions of G–GECO1 to Orai3, an alternative method of activating channel activity with 2-APB in the absence of store depletion revealed a rapid and diffuse increase in fluorescence (Fig. 1*I*). GECI–Orai fusions offer a flexible approach to optically monitor Orai channel activity in transfected cells.

Detection of Unitary Ca^{2+} Signals by Optical Recording at Diffraction-Limited Spots. We noted that the availability of these probes for imaging Orai1-associated Ca^{2+} influx might present an opportunity to optically record from single Orai1 channels. Ca^{2+}-bound G–GECO1 is about half as bright as the green fluorescent protein EGFP (19). Because a fully activated hexamer should be as bright as three EGFP molecules, a microscope capable of imaging single fluorescent proteins should be able to image activation of a single Orai1 channel. In this case, construct function, and not single-channel brightness, should be the limiting factor in optically recording from single Orai1 channels.

HEK 293A cells were transfected with G–GECO1–Orai1 using a previously established, low-expression protocol that results in clearly resolved single Orai1 channels in the basal PM (20). Cells were cotransfected with the CAD fragment of STIM1 fused to the red fluorescent protein mCherry and imaged using TIRF microscopy 3–6 h after transfection. Candidate transfected cells were identified by low expression of mCherry–CAD, and these were imaged at 10 frames per second in 2 Ca. Occasional cells exhibited sporadic green fluorescence transients the size of diffraction-limited spots and the brightness of a few activated G–GECO1 proteins (Fig. 2*A*). A total of 94 transients from four cells were selected for analysis. Transients typically rose to a maximum within 100–200 ms and fell into two classes according to duration. Briefer transients (n = 58) lasted only a few hundred milliseconds, and these were termed "flickers" (Fig. 2 *D* and *F* and Fig. S4 *A–F*). The intensity of many flickers rose to a characteristic level. Longer transients (n = 36) lasted from ~1 to several seconds (Fig. 2*E* and Fig. S4 *G–L*).

PHYSIOLOGY

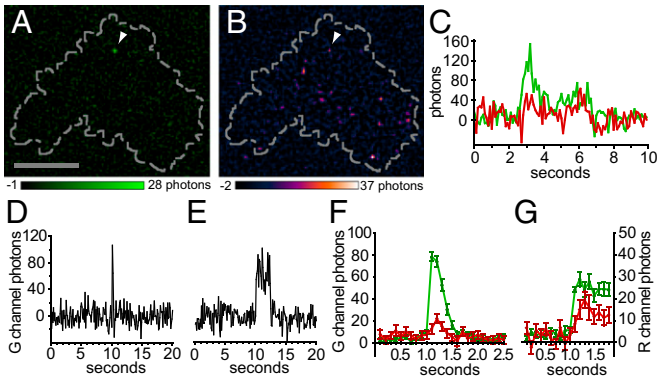

Fig. 2. Discrete G–GECO1–Orai1 fluorescence transients activated by low-level CAD expression are candidate single-channel responses. (*A* and *B*) TIRF images of a HEK 293A cell cotransfected with low levels of G–GECO1–Orai1 (*A*) and mCherry–CAD (pseudocolored in *B*). Arrowhead in *A* indicates a single green fluorescence transient present at the basal surface of the cell (indicated by the dashed line). Note the presence of a fluorescence transient in the corresponding position (arrowhead) in the simultaneously acquired red channel (*B*). (Scale bar, 10 μm.) (*C*) Plots of green (G channel) and red (R channel) fluorescence over time for the transient indicated in *A* and *B*. (*D* and *E*) Example traces of short (flickers, *D*) and long (pulses, *E*) fluorescence transients. (*F* and *G*) Rises in G–GECO1–Orai1 fluorescence are accompanied by corresponding rises in mCherry–CAD fluorescence. Traces were aligned by the rise in green fluorescence and the mean green and red channel fluorescence intensity was plotted versus time for flickers (*F*; $n = 58$) and pulses (*G*; $n = 27$). Error bars indicate ± SEM.

These were termed "pulses." The shape of many traces, with rapid rise and fall, was reminiscent of single channels recorded by electrophysiology. Separate populations of flickers and pulses could be distinguished by plotting the cumulative distribution of transient length (Fig. S5). Fluorescent spots indicative of Orai1 fluorescent transients were more frequent within the footprint of analyzed cells than outside them ($P < 0.0001$, χ^2 test).

In some cases the position of these green fluorescent G–GECO1–Orai1 transients corresponded to the position of a readily apparent red fluorescent mCherry–CAD transient (Fig. 2*B*), and a clear temporal correspondence could be seen between the signals (Fig. 2*C*). If these candidate Ca^{2+} influx events were systematically caused by CAD binding, a rise in colocalized mCherry–CAD fluorescence would accompany them. When traces of G–GECO1–Orai1 were aligned by the rise in green fluorescence (Fig. 2 *F* and *G*), red mCherry–CAD fluorescence increased relative to baseline (for both flickers and pulses, $P < 0.0001$, paired *T* test). A total of 50% of G–GECO1–Orai1 transients (95% confidence interval of 36–62%) were accompanied by a detectable increase in mCherry–CAD fluorescence. mCherry–CAD and G–GECO1–Orai1 fluorescence rose simultaneously, although the magnitude of the mCherry–CAD signal in the first 100-ms image frame was small. These observations are consistent with CAD binding to individual G–GECO1–Orai1 channels in the membrane, resulting in rapid channel opening within 100 ms. Of note, mCherry–CAD fluorescence continued to rise after the onset of the G–GECO1–Orai1 transient, reaching a peak 100 ms (flickers) to 200 ms (pulses) later (Fig. 2 *F* and *G*). However, photobleaching limits the magnitude and temporal resolution of the measured mCherry–CAD signals (*SI Materials and Methods*).

The low frequency of G–GECO1–Orai1 fluorescence transients seen in these experiments (~1 every 5–10 s) precluded detailed physiological characterization. However, higher expression levels of CAD (~20-fold greater) raised the frequency of G–GECO1–Orai1 fluorescence transients to levels suitable for testing (~100-fold greater). Experiments were performed with fusions of G–GECO1.2 to wild-type Orai1 (WT) as well as Orai1 containing Y80E, a mutation that lacks Ca^{2+}-dependent fast inactivation (21). G–GECO1.2–Orai1 was chosen for its higher K_d (1,150 nM versus 750 nM for G–GECO1) (19), which is expected to reduce background response to resting Ca^{2+} levels. Shifting from 0.1 to 2 mM extracellular Ca^{2+} led to the essentially immediate appearance of discrete G–GECO1.2–Orai1 fluorescence transients (Fig. 3 *A* and *B*). As in the previous low-CAD experiments, these transients were the size of diffraction-limited spots and the brightness of a few activated G–GECO1.2 proteins. Transients were widely distributed across the basal plasma membrane (Fig. S6). The rise in the fluorescence of cell footprints (Fig. 3 *C* and *D*) and the number of identified spots (Fig. 3 *E* and *F*) document the onset of single-channel responses in aggregate upon shift to 2 mM Ca^{2}. Shift to 0 mM Ca^{2+} rapidly reversed these signals. Addition of the trivalent cation La^{3+} blocked subsequent response to 2 mM Ca^{2+}. The rise in the number of fluorescence spots upon shift to 2 mM Ca^{2+} corresponded to a rise in the frequency of identified fluorescence transients that was well above background. For example, for the cell responses graphed in Fig. 3, patterns of fluorescence corresponding to flickers were observed 30-fold (Y80E) and 600-fold (WT) more frequently than expected by chance. Because of the size, intensity, trace shape, frequency, distribution, physiological characteristics, and association with CAD binding, we conclude that G–GECO1– and G–GECO1.2–Orai1 fluorescence transients correspond to single-channel Orai1 responses.

Fluctuations in Optical Single-Channel Recordings. Examination of temporally smoothed single-channel traces taken shortly after

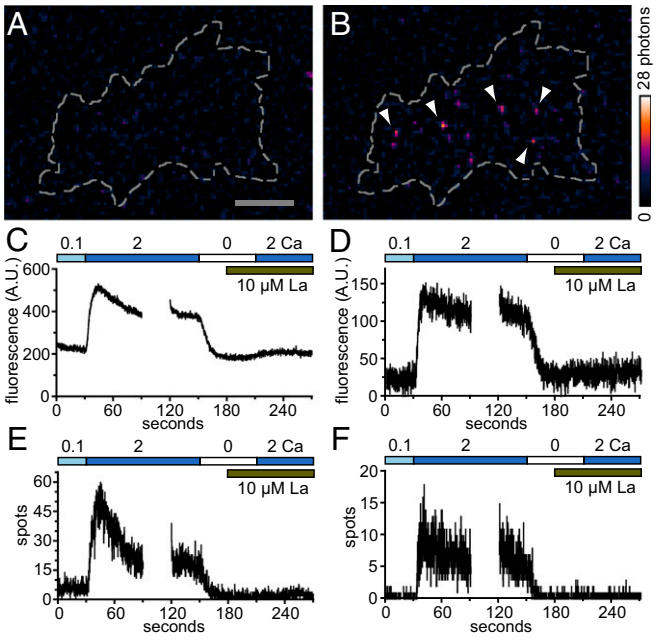

Fig. 3. Discrete G–GECO1.2–Orai1 fluorescence transients activated by high-level CAD expression exhibit physiological characteristics of Orai1 channels. (*A* and *B*) TIRF images of a HEK 293A cell cotransfected with low levels of G–GECO1.2–Orai1 Y80E and high levels of CAD in 0.1 Ca (*A*) and 2 s later after shift to 2 Ca (*B*). Arrowheads indicate selected fluorescence transients present at the basal surface of the cell (indicated by the dashed line). (Scale bar, 5 μm.) (*C* and *D*) Time courses of mean green fluorescence (arbitrary units, A.U.) of the cell basal surface of HEK 293A cells transiently cotransfected with either wild-type Orai1 (*C*) or Y80E (*D*) G–GECO1.2–Orai1 and high levels of CAD. (*E* and *F*) Time course of the number of fluorescent spots identified from the cell basal surface of HEK 293A cells transiently cotransfected with either WT (*E*) or Y80E (*F*) G–GECO1.2–Orai1 and high levels of CAD. *C* and *E* and *D* and *F* are individual cell responses representative of $n = 3$ and $n = 5$ cells, respectively.

shift to 2 mM Ca^{2+} reveals that responses fluctuate markedly over time (Fig. 4 *A* and *B* and Fig. S7 *A–F*). Traces were typically composed of multiple pulses, each ∼1–2 s long and spaced by brief pauses of <1 s. Responses typically lasted from 3 to 10 s. Consecutive pulses often shared a characteristic size, shape, and interpulse interval (Fig. 4 *A* and *B* and Fig. S7 *A–F*). Occasionally, stepwise increases in the intensity of pulses were observed, consistent with stepwise activation of individual G–GECO1.2 molecules tethered to the same channel (Fig. S7 *G* and *H*). In many cases, the intensity of pulses decreased to baseline after each fluctuation. Whereas most responses fluctuated over time, unitary pulses and flickers were observed as well (Fig. S7 *I–L*). Some open channels moved slowly in the plasma membrane, although the dramatic fluctuations in intensity precluded tracking. On the whole, channels exhibited consistent responses incompatible with large-scale movement-induced variations in signal intensity. This pattern of movement is compatible with restricted diffusion of channels within membrane "corrals" similar in size to our regions of interest (22). Single-particle tracking of EGFP-labeled Orai1 channels coexpressed with CAD indicates that some Orai1 channels are confined in this way over periods of several seconds (Fig. S8).

Averaging of pulses aligned by their rise should reveal whether fluctuations in intensity are periodic. We reasoned that we would obtain better alignment if we selected traces with a clear and discrete rise, consistent with resting, closed-state channels newly opened by binding of CAD. When these "clean" G–GECO1.2–Orai1 pulses (for example, Fig. 4*A*) are aligned, the average trace exhibits a clear periodicity of ∼1.5 s (Fig. 4*C*; $n = 14$). Oscillations were not synchronized across a given cell. Averaging pulses aligned by absolute time did not reveal the large fluctuations seen in individual pulses, and the small fluctuations observed were not systematically aligned with pulse rise or fall (Fig. S9 *A* and *B*). Comparison by conversion of traces into adjacent, intensity-mapped image strips, in the manner of Demuro and Parker (14), did not reveal a clear alignment of trace peaks or troughs (Fig. S9 *C* and *D*). Moreover, single EGFP-labeled Orai1 channels coexpressed with CAD did not exhibit large fluctuations in intensity, suggesting that repetitive movements of the membrane along the *z* axis are not responsible for fluctuations in G–GECO–Orai1 output (Fig. S8). Notably, the pulses from low CAD cells, when aligned, produce an average trace that also exhibits a clear periodicity of ∼1.5 s (Fig. 4*D*; $n = 27$). In this case periodicity is seen for mCherry–CAD as well, although the amplitude is smaller. Starting with the second mCherry–CAD peak, these peaks precede the G–GECO1–Orai1 peaks by ∼0.5 s. These responses are consistent with the periodic opening and closing of independent single Orai1 channels.

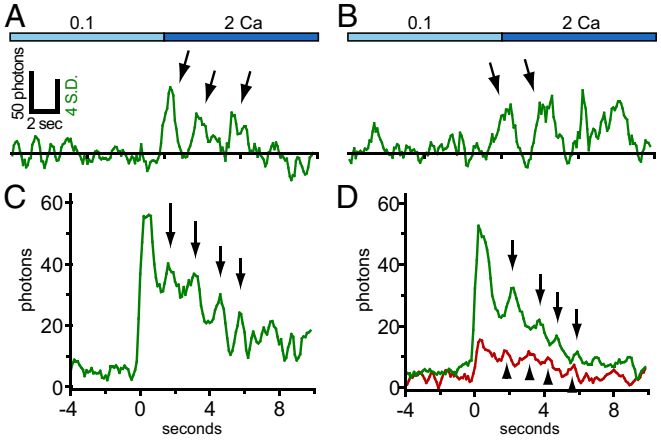

Fig. 4. Fluctuations in single-channel optical recordings. (*A* and *B*) Example single channel traces of G–GECO1.2–Orai1 WT upon shift from 0.1 to 2 Ca. Arrows in *A* and *B* indicate fluctuations in the fluorescence traces. The right vertical scale bar indicates 4 SD above the mean cell basal surface fluorescence. Traces are four-frame moving averages and are aligned by the initial rise in fluorescence after shift to 2 Ca. (*C* and *D*) Averaged aligned pulses exhibit apparently periodic fluctuations. (*C*) Pulses ($n = 14$) from high-level CAD-expressing cells ($n = 3$) possessing "clean" rises were aligned by the initial rise and averaged, and the mean fluorescence intensity was plotted versus time. Arrows indicate consecutive peaks. (*D*) Pulses ($n = 27$) from low-level CAD-expressing cells ($n = 4$) were aligned by the initial rise and the mean fluorescence intensity was plotted versus time. Downward arrows indicate consecutive peaks in the GECO1–Orai1 WT trace and upward arrowheads indicate offset consecutive peaks in the mCherry–CAD trace. Plots are four-frame moving averages.

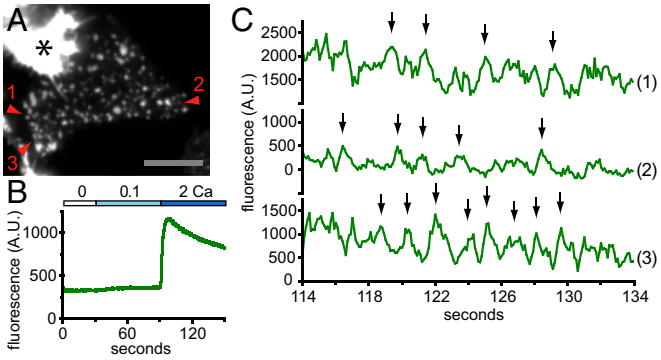

Fig. 5. Single-channel activity in Orai1 puncta. (*A*) Green channel TIRF image of a HEK 293A cell cotransfected with G–GECO1.2–Orai1 and STIM1 after treatment with 2 μM TG. Average of 200 consecutive frames taken for the time period plotted in *C*. Red arrowheads indicate puncta plotted in *C*. (Scale bar, 10 μM.) Asterisk indicates a brightly fluorescent adjacent cell. (*B*) Time course of mean G–GECO1.2–Orai1 fluorescence of the cell footprint (in arbitrary units, A.U.) imaged at 10 frames per second. (*C*) Single-pixel intensity records of G–GECO1.2–Orai1 at the center of a punctum (*1*), at the edge of a dim punctum (*2*), and in a punctum that exhibits periodic fluorescence intensity fluctuations (*3*). Arrows indicate characteristic peaks repeated in each trace. Time corresponds to the plot in *B*. Traces are four-frame moving averages. Responses taken from one of $n = 3$ cells.

We sought to determine whether the fluctuations in Ca^{2+} influx we observed for single channels gated by CAD occurred for channels assembled into puncta and gated by full-length STIM1. HEK 293A cells were cotransfected with G–GECO1.2–Orai1 and STIM1, and clustering of Orai1 into puncta was initiated through store depletion using TG in 0 mM Ca^{2+} (Fig. 5*A*). Puncta imaged at high speed (10 frames per second) exhibited the expected rise in fluorescence upon shift from 0.1 to 2 mM Ca^{2+} (Fig. 5*B*). Cells possessing roughly 500–1,000 open G–GECO1.2–Orai1 channels per footprint, distributed among ∼100–150 puncta, were chosen for analysis. Single-pixel traces from puncta fluctuated markedly (Fig. 5*C* and Fig. S10). Upon application of a four-frame moving average filter, deviations lasting ∼1.5 s could be detected (Fig. 5*C*, trace 1). These features are reminiscent of fluctuating single-channel responses observed in macroscopic whole-cell currents. Similar features could be seen in single-pixel traces taken from the edge of dim puncta, and their emergence from baseline marks them as presumptive single-unit events (Fig. 5*C*, trace 2 and Fig. S10, traces 4, 5, and 7). More extended bouts of periodic fluctuations were observed as well (Fig. 5*C*, trace 3 and Fig. S10, traces 1–3 and 6). Puncta responses across the cell were not synchronized (compare Fig. 5*C*, traces 1–3, Fig. S10, traces 1–5, and Fig. S10, traces 6–7). All three experimental configurations, (*i*) low open probability due to low CAD expression; (*ii*) high open probability due to high CAD expression; and (*iii*) Orai1 puncta gated by STIM1, feature repetitive fluctuations in single-channel output.

PHYSIOLOGY

Discussion

Orai channels in the PM are gated by direct physical contact of STIM C termini extending from the cytoplasmic face of the ER. This subcellular organization, combined with the extremely small conductance of Orai channels, has limited progress in understanding these channels and their contributions to cell signaling. The method we introduce here offers new approaches to probing Orai function in puncta and at the single-channel level. GECI–Orai fusions selectively and directly report Orai channel activity, and we use these to record from single Orai1 channels for the first time to our knowledge. Our results reveal an unexpected complexity in Orai1 gating dynamics.

Orai1 channel activity was imaged directly at high dynamic range in cells transfected with GECI–Orai fusions. By electrophysiology, fusion to GECIs resulted in little or no change in Orai1 function. These fusions target appropriately, report Ca^{2+} influx in HEK 293A cells and human T cells, and report activation of Orai channels by different mechanisms: STIM-dependent activation of Orai1 and STIM-independent activation of Orai3 by 2-APB. This approach should identify restricted, asynchronous, or transient Orai-mediated signaling events in a variety of cells. Indeed, we identify stereotyped fluctuations in Ca^{2+} influx that varied asynchronously between puncta of the same cell. Using TIRF microscopy, the sensitivity of this approach extends to nanodomains consisting of only a single channel open for a few hundred milliseconds.

Several lines of evidence indicate that fluorescent transients found in cells expressing GECO–Orai1 and CAD correspond to single-channel opening events. These include their size, intensity, trace shape, frequency, distribution, physiological characteristics, and association with CAD binding. To what extent are our recorded traces an accurate readout of channel activity? Clearly, our understanding is limited by uncertainty in the response function of GECO–Orai1 fusions. For example, these fusions detect the existence of an entire class of responses, flickers, as short of 200–300 ms, which is substantially shorter than predicted based upon the in vitro off rates measured for G–GECO1 and G–GECO1.2 alone (for both, $0.7 \cdot s^{-1}$; *SI Materials and Methods*) (19). Changes in GECI performance have been attributed to protein fusion or subcellular environment in other studies as well (17, 23). Despite the uncertainty, these traces can be used to support or constrain models of channel activity and gating that involve large, long-lasting, or repetitive Ca^{2+} fluxes.

We have named our method of optical patch clamping, genetically targeted single-channel optical recording (GT-SCOR). Previously developed approaches use chemical Ca^{2+} indicators loaded into the cytoplasm, such as Fluo-4, to detect influx of Ca^{2+} from individual channels. In GT-SCOR, channels are targeted directly by fusion to a GECI, resulting in a 1:1 covalent association of channel subunits and sensors positioned nanometers from the pore. This arrangement is exquisitely sensitive; indeed, we find robust Orai1 single-channel responses, whereas a similar Fluo-4 based, optical patch-clamping study in *Xenopus* oocytes was unable to detect sites of store operated Ca^{2+} influx that occur at clusters of Orai channels (24). However, Fluo-4–based optical patch clamping has inherent advantages, including essentially no photobleaching, the ability to image channels without tagging, and the ability to image currents much faster (up to 500 Hz) than GT-SCOR.

Fluorescence transients fell into two classes according to duration: shorter flickers and longer pulses. Do these two classes correspond to two modes of channel gating? At the level of elemental gating movements, they may not be different. Pulses could be made up of bursts of flickers, and this possibility might be detected by imaging more rapidly. Nevertheless, the extended temporal correlations in intensity and duration found in pulses, and missing from more unitary flickers, support the existence of two functional modes of Orai1 channel gating.

Structural information provided by the crystal structure of *Drosophila* Orai (7) and the NMR structure of the cytoplasmic coiled-coil portion of STIM1 (25) has led to the hypothesis that STIM1 holds Orai1 in an open state. If this hypothesis is correct, then continuous STIM1 binding is necessary to keep the channel open. Alternatively, STIM1 binding may be necessary to initiate channel opening, but not to maintain the open state. Our data support the former model: for pulses, binding persists for many hundreds of milliseconds after channel opening (Figs. 2*G* and 4*D*).

Most low-CAD G–GECO1–Orai1 transients rise within a single 100-ms frame (Fig. 2 *F* and *G*). CAD binding, however, occurs more progressively, reaching a peak 100 ms (for flickers) to 200 ms (for pulses) later. These data point to the existence of a second phase of CAD binding that occurs after channel opening. The ratio of STIM1:Orai1 determines many channel properties (10–13); this second phase of binding likely changes CAD:Orai1 stoichiometry and Orai1 conducting state. In addition, these two phases of CAD binding delineate steps in a molecular activation/deactivation cascade that accompanies channel gating.

We identified fluctuations of G–GECO1.2–Orai1 signal in puncta formed by coexpression of STIM1 and treatment with TG. At the edge of dim puncta, signals of similar intensity and duration were found rising from baseline. The most straightforward explanation is that they are unitary Orai1 channel events. Given that their trace shape, duration, and period are similar to short pulses, gating by CAD appears to resemble gating by STIM1 in essential aspects.

All three experimental configurations reveal fluctuations in the fluorescence output of single channels with a ∼1.5-s period. The similarity between consecutive large pulses that emerge from baseline indicates that the output of multiple GECO proteins rise and fall in a coordinated manner. Whereas the output of fluorescent proteins "blink" on a variety of time scales, we know of no photophysical process that would lead to a coordinated and periodic output by fluorescent proteins (26). Moreover, a periodic output is not consistent with the expected declining exponential distribution of GECO on state lifetime either. We acknowledge that periodic changes in channel structure or local pH might lead to periodic inactivation of the GECO probes. However, notably, CAD binding fluctuates with a period similar to that seen for Orai1, although to a lesser degree. Taken together, these arguments support the assertion that periodic oscillations in fluorescence transients are due to periodic fluctuation in the activity of single Orai1 channels.

Additional experiments are required to determine the origin of these fluctuations. The outputs of unitary events are not synchronized across puncta, and single-channel responses driven by CAD show no clear evidence of coordination. Fluctuations in Orai1 activity persist in the presence of a mutation that blocks Ca^{2+}-dependent fast inactivation, although other unidentified Ca^{2+}-dependent processes might contribute. Nevertheless, the periodicity in CAD binding makes CAD/STIM1 a prime candidate for driving Orai1 oscillations. Fluctuations in CAD binding are out of phase with and precede Orai1 activity peaks. Given the similarity in output of the three different experimental configurations, we suggest that single Orai1 channels gated by CAD/STIM1 may act as intrinsic oscillators. Oscillations such as these, with a defined period, are due to multistep negative feedback mechanisms and differ mechanistically from stochastically fluctuating responses (27, 28).

The oscillations we observe in Orai1 single-channel activity do not appear to be the output of some upstream signal, but instead a property of the channel and its subcellular environment. This presents difficulties in interpreting the potential consequences, and contributions, of these fluctuations to cellular signaling. Their period is shorter than widely studied IP_3-dependent Ca^{2+} oscillations (tens to hundreds of seconds). Orai1 channels in puncta are surrounded by dozens to hundreds of identical channels that appear to be unsynchronized. This arrangement might be

expected to mask single-channel fluctuations. In the absence of coordination, fluctuations would still remain distinct in small puncta with few active channels, as seen in dim puncta in HEK 293A cells. Alternatively, in other cell types, Orai1 single-channel fluctuations may be linked to generate much larger oscillating signals, which might allow for adaptation-dependent readout of Orai1 activity (29).

These first single-channel recordings for Orai1 confirm basic aspects of Orai1 gating models: direct activation and open state maintenance by CAD/STIM1. They support also an unexpected complexity in gating dynamics, with two functional modes, a second phase of CAD/STIM1 binding after channel opening, and an unexpected periodicity in Orai1 single-channel currents. More generally, this work opens the door for functional studies at the single-molecule level on a wide range of Ca^{2+}-dependent signaling mechanisms.

Materials and Methods

Cell Culture and Reagents. HEK 293A cells (Invitrogen) were cultured as in ref. 20, and human T cells were isolated and transfected as in ref. 30.

Molecular Biology and Transfection Conditions. Plasmid construction is detailed in *SI Materials and Methods*. Transfections for single-molecule assays were performed as described in ref. 20.

Microscopy and Imaging. TIRF and near TIRF imaging were performed on an Olympus IX81 microscope with a home-built TIRF illumination system, Olympus 60× 1.45 N.A. PlanApoN TIRF objective, Photometrics DualView2 image splitter, Photometrics Evolve 512 EMCCD camera, 488-nm Argon ion laser, and a 561-nm solid state laser. See *SI Materials and Methods* for further details.

Image Processing, Analysis, and Statistical Testing. Image processing and measurement were performed using ImageJ 1.41; intensity calculations were performed in Microsoft Excel; and statistical testing, SEM calculation, and graphing were performed in Prism 4 (GraphPad Software). For quantification procedures related to signal and noise, see *SI Materials and Methods*.

Whole-Cell Recording. Whole-cell recordings were done on transfected HEK 293A cells as described previously (31, 32), using procedures and solutions described in *SI Materials and Methods*.

ACKNOWLEDGMENTS. We thank Luette Forrest and Tobias X. Dong for isolating and transfecting human T cells, Olga Safrina for creating the DNA fusion construct G–GECO1.2–Orai1 Y80E, and Ian Parker for advice on total internal reflectance fluorescence microscopy and comments on the manuscript. This work is supported by NIH Grant R01 NS-14609 (to M.D.C.). Human blood was prepared using support from the National Center for Research Resources and the National Center for Advancing Translational Sciences (NIH Grant UL1 TR000153).

1. Clapham DE (2007) Calcium signaling. *Cell* 131(6):1047–1058.
2. Parekh AB, Putney JW, Jr (2005) Store-operated calcium channels. *Physiol Rev* 85(2):757–810.
3. Amcheslavsky A, et al. (2015) Molecular biophysics of Orai store-operated Ca2+ channels. *Biophys J* 108(2):237–246.
4. Prakriya M, Lewis RS (2015) Store-operated calcium channels. *Physiol Rev* 95(4):1383–1436.
5. Shaw PJ, Feske S (2012) Regulation of lymphocyte function by ORAI and STIM proteins in infection and autoimmunity. *J Physiol* 590(Pt 17):4157–4167.
6. Cahalan MD, Chandy KG (2009) The functional network of ion channels in T lymphocytes. *Immunol Rev* 231(1):59–87.
7. Hou X, Pedi L, Diver MM, Long SB (2012) Crystal structure of the calcium release-activated calcium channel Orai. *Science* 338(6112):1308–1313.
8. Park CY, et al. (2009) STIM1 clusters and activates CRAC channels via direct binding of a cytosolic domain to Orai1. *Cell* 136(5):876–890.
9. Yuan JP, et al. (2009) SOAR and the polybasic STIM1 domains gate and regulate Orai channels. *Nat Cell Biol* 11(3):337–343.
10. Hoover PJ, Lewis RS (2011) Stoichiometric requirements for trapping and gating of Ca2+ release-activated Ca2+ (CRAC) channels by stromal interaction molecule 1 (STIM1). *Proc Natl Acad Sci USA* 108(32):13299–13304.
11. McNally BA, Somasundaram A, Yamashita M, Prakriya M (2012) Gated regulation of CRAC channel ion selectivity by STIM1. *Nature* 482(7384):241–245.
12. Scrimgeour N, Litjens T, Ma L, Barritt GJ, Rychkov GY (2009) Properties of Orai1 mediated store-operated current depend on the expression levels of STIM1 and Orai1 proteins. *J Physiol* 587(Pt 12):2903–2918.
13. Li Z, et al. (2011) Graded activation of CRAC channel by binding of different numbers of STIM1 to Orai1 subunits. *Cell Res* 21(2):305–315.
14. Demuro A, Parker I (2005) "Optical patch-clamping": Single-channel recording by imaging Ca2+ flux through individual muscle acetylcholine receptor channels. *J Gen Physiol* 126(3):179–192.
15. Zweifach A, Lewis RS (1993) Mitogen-regulated Ca2+ current of T lymphocytes is activated by depletion of intracellular Ca2+ stores. *Proc Natl Acad Sci USA* 90(13):6295–6299.
16. Richler E, Chaumont S, Shigetomi E, Sagasti A, Khakh BS (2008) Tracking transmitter-gated P2X cation channel activation in vitro and in vivo. *Nat Methods* 5(1):87–93.
17. Tay LH, et al. (2012) Nanodomain Ca^{2+} of Ca^{2+} channels detected by a tethered genetically encoded Ca^{2+} sensor. *Nat Commun* 3:778.
18. Chen TW, et al. (2013) Ultrasensitive fluorescent proteins for imaging neuronal activity. *Nature* 499(7458):295–300.
19. Zhao Y, et al. (2011) An expanded palette of genetically encoded Ca^{2+} indicators. *Science* 333(6051):1888–1891.
20. Demuro A, et al. (2011) Subunit stoichiometry of human Orai1 and Orai3 channels in closed and open states. *Proc Natl Acad Sci USA* 108(43):17832–17837.
21. Mullins FM, Park CY, Dolmetsch RE, Lewis RS (2009) STIM1 and calmodulin interact with Orai1 to induce Ca2+-dependent inactivation of CRAC channels. *Proc Natl Acad Sci USA* 106(36):15495–15500.
22. Kusumi A, et al. (2005) Paradigm shift of the plasma membrane concept from the two-dimensional continuum fluid to the partitioned fluid: High-speed single-molecule tracking of membrane molecules. *Annu Rev Biophys Biomol Struct* 34:351–378.
23. Heim N, Griesbeck O (2004) Genetically encoded indicators of cellular calcium dynamics based on troponin C and green fluorescent protein. *J Biol Chem* 279(14):14280–14286.
24. Demuro A, Smith M, Parker I (2011) Single-channel Ca(2+) imaging implicates Aβ1-42 amyloid pores in Alzheimer's disease pathology. *J Cell Biol* 195(3):515–524.
25. Stathopulos PB, et al. (2013) STIM1/Orai1 coiled-coil interplay in the regulation of store-operated calcium entry. *Nat Commun* 4:2963.
26. Ha T, Tinnefeld P (2012) Photophysics of fluorescent probes for single-molecule biophysics and super-resolution imaging. *Annu Rev Phys Chem* 63:595–617.
27. Novák B, Tyson JJ (2008) Design principles of biochemical oscillators. *Nat Rev Mol Cell Biol* 9(12):981–991.
28. Skupin A, et al. (2008) How does intracellular Ca2+ oscillate: By chance or by the clock? *Biophys J* 94(6):2404–2411.
29. Behar M, Dohlman HG, Elston TC (2007) Kinetic insulation as an effective mechanism for achieving pathway specificity in intracellular signaling networks. *Proc Natl Acad Sci USA* 104(41):16146–16151.
30. Greenberg ML, et al. (2013) Orai1 function is essential for T cell homing to lymph nodes. *J Immunol* 190(7):3197–3206.
31. Yeromin AV, et al. (2006) Molecular identification of the CRAC channel by altered ion selectivity in a mutant of Orai. *Nature* 443(7108):226–229.
32. Zhang SL, et al. (2008) Store-dependent and -independent modes regulating Ca2+ release-activated Ca2+ channel activity of human Orai1 and Orai3. *J Biol Chem* 283(25):17662–17671.
33. Lioudyno MI, et al. (2008) Orai1 and STIM1 move to the immunological synapse and are up-regulated during T cell activation. *Proc Natl Acad Sci USA* 105(6):2011–2016.
34. Amcheslavsky A, Safrina O, Cahalan MD (2013) Orai3 TM3 point mutation G158C alters kinetics of 2-APB-induced gating by disulfide bridge formation with TM2 C101. *J Gen Physiol* 142(4):405–412.
35. Amcheslavsky A, Safrina O, Cahalan MD (2014) State-dependent block of Orai3 TM1 and TM3 cysteine mutants: Insights into 2-APB activation. *J Gen Physiol* 143(5):621–631.
36. Ellefsen KL, Dynes JL, Parker I (2015) Spinning-spot shadowless TIRF microscopy. *PLoS One* 10(8):e0136055.
37. Sun XR, et al. (2013) Fast GCaMPs for improved tracking of neuronal activity. *Nat Commun* 4:2170.
38. Sage D, Neumann FR, Hediger F, Gasser SM, Unser M (2005) Automatic tracking of individual fluorescence particles: Application to the study of chromosome dynamics. *IEEE Trans Image Process* 14(9):1372–1383.
39. Dynes JL, Steward O (2012) Arc mRNA docks precisely at the base of individual dendritic spines indicating the existence of a specialized microdomain for synapse-specific mRNA translation. *J Comp Neurol* 520(14):3105–3119.
40. Chenouard N, et al. (2014) Objective comparison of particle tracking methods. *Nat Methods* 11(3):281–289.
41. Jaqaman K, et al. (2008) Robust single-particle tracking in live-cell time-lapse sequences. *Nat Methods* 5(8):695–702.
42. Wu MM, Covington ED, Lewis RS (2014) Single-molecule analysis of diffusion and trapping of STIM1 and Orai1 at endoplasmic reticulum-plasma membrane junctions. *Mol Biol Cell* 25(22):3672–3685.